Regular Arrays of Monodisperse Platinum/Erbium Disilicide Core−Shell Nanowires and Nanoparticles on Si(001) via a Self−Assembled Template

6 AUTHORS, INCLUDING:

Jiun-Pyng You
University of California, Irvine
16 PUBLICATIONS **223** CITATIONS

Ju H Choi
Korea Photonics Technology Institute
28 PUBLICATIONS **344** CITATIONS

Stan Williams
Hewlett-Packard Inc.
510 PUBLICATIONS **22,544** CITATIONS

Regina Ragan
University of California, Irvine
64 PUBLICATIONS **542** CITATIONS

Regular Arrays of Monodisperse Platinum/Erbium Disilicide Core−Shell Nanowires and Nanoparticles on Si(001) via a Self-Assembled Template

Jiun Pyng You,[†] Ju H. Choi,[†] Sehun Kim,[‡] Xuema Li,[§] R. Stanley Williams,[§] and Regina Ragan*,[†]

Department of Chemical Engineering and Materials Science, University of California, Irvine, California 92697, Department of Chemistry, Korea Advanced Institute of Science and Technology, 373-1 Geseong-dong, Yuseong-gu, Daejeon, 305-701, Korea, and Quantum Science Research Group, Hewlett-Packard Laboratories, MS 1123, 1501 Page Mill Road, Palo Alto, California 94304

ABSTRACT

We have developed a process for fabricating monodisperse noble metal/rare earth disilicide core−shell nanoparticles and nanowires in regular arrays on Si(001) with a density of 5×10^{10} / cm², and over areas >1 mm². Pt deposited via physical vapor deposition on a self-assembled rare earth disilicide nanowire template combined with reactive ion etching produces arrays of nanostructures. SEM images demonstrate the ability to select nanowires or nanoparticles as a function of Pt coverage. Statistical analysis of images of Pt nanoparticle arrays yield a mean feature size of 8 nm with a size variation of ±0.9 nm and interparticle spacing of approximately 15 nm.

Metal nanostructures have demonstrated the capacity for single-molecule detection limits in plasmon resonance biosensors: chemical selectivity, higher performance in catalytic processes than their bulk counterparts, and the transport of electromagnetic energy along particle chains, to name a few examples. In this letter, we address one of the most significant challenges to technological developments that capitalize on unique properties of metal nanoparticles (NPs) and nanowires (NWs): the fabrication of high-density nanostructure arrays with monodisperse size, shape, and interparticle spacing using a low-cost and high-throughput technique. In noble metal nanostructures, the plasmon resonance frequency strongly depends on size,[1] shape,[2] and interparticle spacing.[3] The strong near-field coupling between closely spaced particles leads to a Raman scattering signal with theoretically predicted enhancement factors of 10^6-10^{14}, affording the possibility of adsorbed single-molecule detection.[4,5] For molecular catalysis, in the case of Pt in bulk form, the catalytic turnover rate is decreased by 6 orders of magnitude after exposure to carbon monoxide, a byproduct of many catalytic reactions.[6,7] In comparison, Pt nanoparticles

having a width on the order of 20 nm have exhibited a significantly lower susceptibility to carbon monoxide poisoning than bulk single-crystal Pt(111) when the turnover rate was measured for ethylene hydrogenation on both platforms.[7] Bimetallic[8−11] and metal/oxide[10,12] core−shell[13,14] nanoparticles with diameters on nanometer length scales exhibit peculiar chemical activity and selectivity in catalytic reactions that are not available in bulk form. In this letter, we discuss a unique Si-compatible fabrication process for dense ordered arrays ($\sim 10^{11}$ cm^{-2}) of metallic nanostructures with monodisperse size and shape, over large area (>1 mm²), and having feature size and interparticle spacing that exceeds state of the art electron-beam lithography that has been developed. Rare earth disilicide (RESi$_{2-x}$) NWs with high aspect ratios,[15] lengths exceeding 1 micrometer and widths less than 5 nm, have been fabricated previously.[16,17] These RESi$_{2-x}$ NWs can be grown successfully on vicinal Si(001) substrates with a miscut of 2−2.5° toward the [110] azimuth.[18−20] The growth of RESi$_{2-x}$ (RESi$_{2-x}$, RE = Dy, Er, Gd) NWs has been attributed to an anisotropic lattice mismatch between the a and c axis of the hexagonal RESi$_{2-x}$ lattice with respect to Si[110],[21] and the NW width is governed by strain.[22] We have shown that deposition of Pt on RESi$_{2-x}$ NWs on Si-(001) renders the highly reactive RESi$_{2-x}$ NW surface air stable.[23] In this letter, we demonstrate the fabrication of Pt/

* Corresponding author. Tel: (949)824-6830. Fax: (949)824-2541. E-mail: rragan@uci.edu.
† University of California.
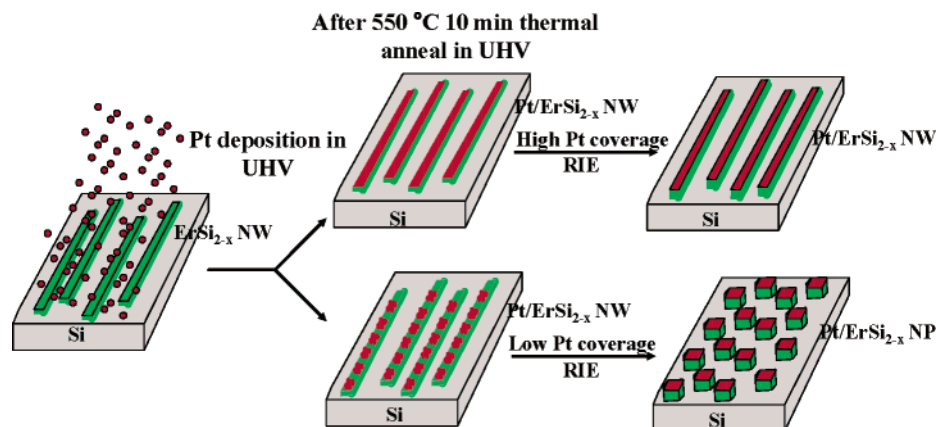‡ Korea Advanced Institute of Science and Technology.
§ Hewlett-Packard Laboratories.

Figure 1. Schematic diagram of the fabrication process of Pt/ErSi$_{2-x}$ NW and NP arrays by Pt deposition at room temperature on ErSi$_{2-x}$ NWs on Si(001) in UHV followed by annealing at 550 °C for 10 min; the resulting nanostructures are defined after RIE as NW or NP arrays resulting from high or low Pt coverage, respectively.

ErSi$_{2-x}$ core−shell NPs and NWs in regular arrays with a mean feature size of 8 nm and having an approximate density of 5×10^{10}/cm^2 over areas greater than 1 mm^2 by using ErSi$_{2-x}$ NWs as a self-assembled template on Si(001). Because this process uses selective aggregation of Pt on a nanowire template, it can be applied to other noble metals such as Au,[24] Pd, and Co in order to fabricate nanostructures for a broad range of applications.

Self-assembled ErSi$_{2-x}$ NW arrays were grown by physical vapor deposition (PVD) of Er on Si(001) in an ultrahigh vacuum (UHV) system with a base pressure of 10^{-10} Torr and a VT Omicron scanning tunneling and atomic force microscope (STM/AFM) attached. The details of ErSi$_{2-x}$ NW growth have been described in detail elsewhere.[25] Following Er deposition at 600 °C and NW formation, PVD of Pt at submonolayer quantities was performed at room temperature and followed by an anneal at 550 °C for 10 min. Scanning tunneling microscopy (STM) images were obtained before and after Pt deposition. All STM images were acquired at room temperature with the VT Omicron STM/AFM. After imaging, samples were removed from UHV and subjected to a reactive ion etch (RIE) using CHF$_3$ gas. A schematic diagram of the fabrication process is shown in Figure 1. Surface morphology was examined by scanning electron microscopy (SEM) and ambient AFM after RIE. SEM imaging using backscattered electrons was performed to achieve atomic contrast on the surface in order to examine the surface distribution of Pt atoms. NP mean size and the size distribution were calculated from SEM images using Fovea Pro (Reindeer Graphics Corp.).

A 500 × 500 nm^2 STM image of ErSi$_{2-x}$ NWs on Si-(001) is shown in Figure 2a. The NWs form along Si[110] and have an average length of 200 nm. A high-resolution STM image is shown in Figure 2b. The $c(2 \times 2)$ surface reconstruction is visible on the NW surface that is characteristic of the hexagonal AlB_2 structure. The 500 × 500 nm^2 STM image of Figure 2c shows the morphology of Pt/ErSi$_{2-x}$/Si(001) NWs after PVD of Pt at room temperature followed by annealing at 550 °C for 10 min. The NW size and shape does not change noticeably; the average feature length and width of NWs are the same before and after Pt
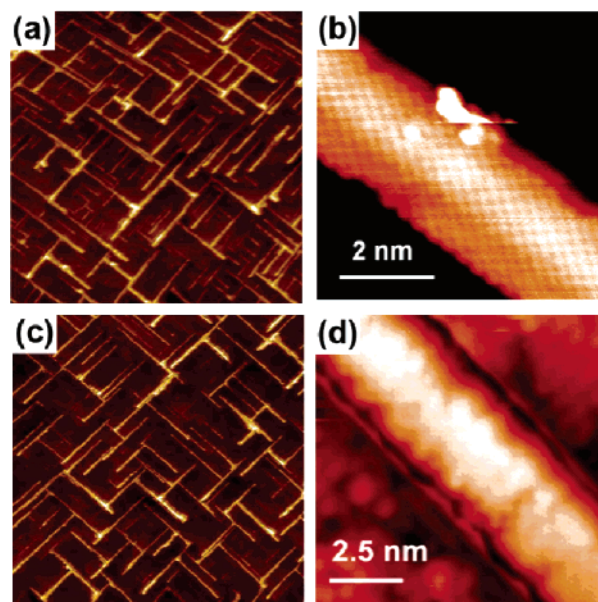

Figure 2. STM images of self-assembled ErSi$_{2-x}$ NWs on Si(001): (a) 500 × 500 nm^2 region; (b) a high-resolution image where the $c(2 \times 2)$ surface reconstruction is visible on the ErSi$_{2-x}$ NW surface. The NW width is approximately 3 nm; (c) 500 × 500 nm^2 region after Pt deposition and thermal annealing at 550 °C for 10 min; (d) and a high-resolution image where the $c(2 \times 2)$ surface reconstruction is no longer observed on the ErSi$_{2-x}$ NW surface after Pt deposition and annealing; however, the Si (2×1) substrate reconstruction is still visible in upper right corner.

deposition. Nevertheless, the $c(2 \times 2)$ surface reconstruction is no longer observed on the nanowire surface, as seen in the STM image of Figure 2d. The 2×1 surface reconstruction is still evident on the Si surface next to the nanowire. The areal density of Pt on this sample surface is 6.78×10^{13}/cm^2 (0.1 ML) as determined from Rutherford backscattering spectroscopy (RBS). Previous research has shown that if Pt coverage on Si(001) is less than 1/6 monolayer (ML) then Pt will induce disorder of the Si 2×1 reconstruction, and if the coverage is greater than 1/6 ML, a $c(4 \times 2)$ and/or $c(4 \times 6)$ can be observed on Si(001).[26]

To gain insight into how Pt atoms are distributed on ErSi$_{2-x}$ NW/Si(001) surfaces, the nanostructure morphology
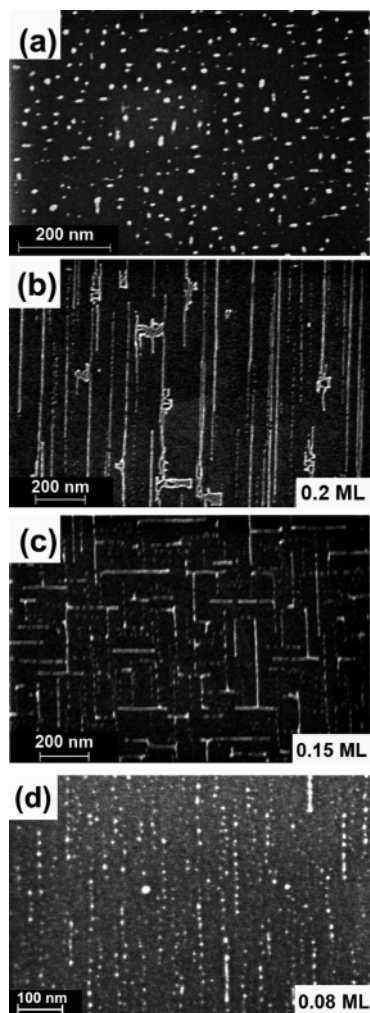
Figure 3. SEM images taken after RIE samples in CHF$_3$ gas for 45s: (a) ErSi$_{2-x}$/Si(001) surface; (b) Pt/ErSi$_{2-x}$/Si(001) surface with 0.2 ML Pt coverage; (c) Pt/ErSi$_{2-x}$/Si(001) surface with 0.15 ML Pt coverage; and (d) Pt/ErSi$_{2-x}$/Si(001) surface with 0.08 ML Pt coverage. (Note that in parts a and c the Si substrate is nominally flat and in parts b and d the vicinal Si surface has a miscut of 2.5° toward the [110] azimuth.)

evolution due to RIE samples in CHF$_3$ gas for 45 s with varying Pt coverage was measured with SEM. The Pt coverage in some cases was extrapolated from a calibration generated by measuring the Pt coverage with RBS for various deposition times at fixed evaporator power. Figure 3a shows a SEM image after RIE of an ErSi$_{2-x}$/Si(001) surface without Pt; the remaining nanostructures resemble rectangular NPs of varying size, and NWs are no longer observed. Figure 3b is a SEM image after a similar RIE process of a Pt/ErSi$_{2-x}$/Si(001) sample with an approximate Pt coverage of 0.2 ML. Most of the NWs are observed to remain 200 nm in length (as observed in STM images taken before RIE) for the sample with 0.2 ML of Pt but not for the sample without Pt. The nanostructure evolution as a function of Pt coverage on Pt/ErSi$_{2-x}$/Si(001) surfaces after the samples undergo similar RIE procedures is shown in Figure 3b−d. After RIE, at approximate Pt coverage of 0.2 ML NWs are predominant, at measured Pt coverage of 0.15 ML NWs and NPs coexist, and at approximate Pt coverage of 0.08 ML NPs are
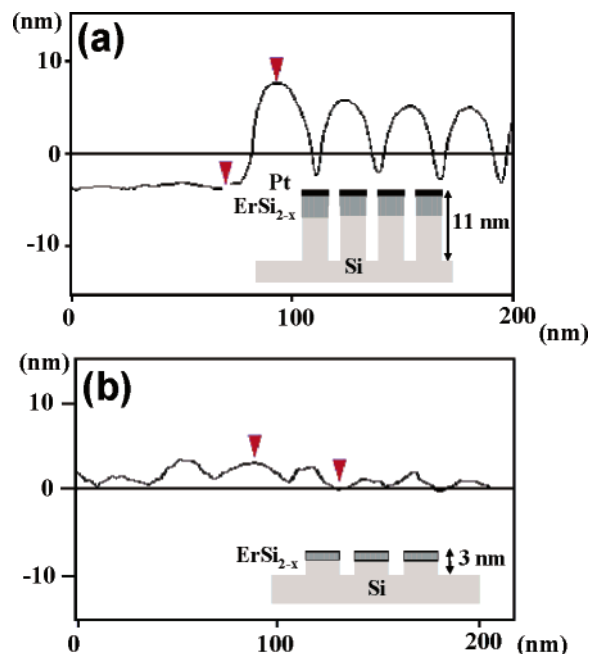

Figure 4. AFM line profiles of samples after RIE of the following: (a) Pt/ErSi$_{2-x}$/Si(001) with 0.1 ML Pt coverage; the average feature height is 11 nm; and (b) ErSi$_{2-x}$/Si(001) without Pt; the average feature height is 3 nm. The insets are schematics of the proposed cross section after RIE with respect to each AFM line profile.

Table 1. Areal Coverage of Nanostructures after RIE[a]

areal coverage of NWs before RIE	areal coverage of Pt after RIE	areal coverage of nanostructure after RIE
20%	0.2 ML*	18%
18%	0.15 ML	15%
11.5−14%	0.08 ML*	2%

[a] The areal coverage correlates with Pt areal coverage as measured/calibrated by RBS analysis. * indicates that the data was estimated from the calibration curve generated from the RBS data of other samples.

predominant. Thus, the nanostructures evolve from NW to NP arrays as Pt coverage decreases.

AFM line profiles give evidence that Pt acts as a more resistant etch mask than ErSi$_{2-x}$ and the Si substrate. Line profiles were taken from AFM images of samples after RIE with and without Pt on ErSi$_{2-x}$/Si(001) and are shown in Figure 4a and b, respectively. The average feature height for Pt/ErSi$_{2-x}$/Si(001) NWs before and after etching are approximately 1 and 11 nm and for ErSi$_{2-x}$/Si(001) NWs that undergo the same processing steps are 1 and 3 nm, respectively. From this data, the Pt-covered surface is more resistant to etching. If we consider the areal coverage of features before and after RIE, then the coverage after RIE is correlated to the Pt coverage as seen in Table 1, thus giving further evidence that Pt is indeed acting as an etch mask.

The atomic numbers of Si, Pt, and Er are 14, 78, and 68, respectively. Thus, compositional contrast between Pt and Si, ErSi$_{2-x}$ and Si, and Pt and ErSi$_{2-x}$ is expected when imaging with backscattered electron due to differences in atomic number.[27] In Figure 5, SEM images of (a) Pt/ErSi$_{2-x}$/
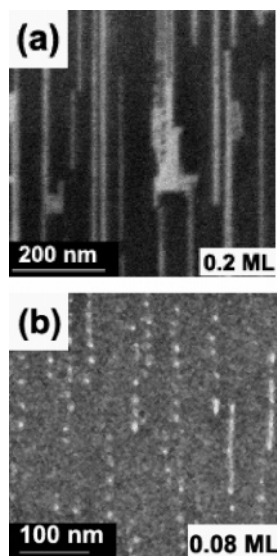
Figure 5. SEM images of (a) the Pt/ErSi$_{2-x}$/Si(001) surface with Pt of 0.2 ML coverage and (b) the Pt/ErSi$_{2-x}$/Si(001) surface with Pt of 0.08 ML coverage after etching both samples in CHF$_3$ gas for 45s. The SEM images were acquired with an acceleration voltage of 2.2 kV with the detector set with a rejection bias of 430−450 V and a working distance of 3 mm in order to reduce the contribution of secondary electrons in order to acquire an image with heightened atomic contrast.

Si(001) samples with a Pt coverage of 0.2 ML and (b) 0.08 ML after RIE are shown. The images were acquired with an acceleration voltage of 2.2 kV and the detector set with a bias of 430−450 V in order to repel low-energy secondary electrons (SE) and image primarily with backscattered electrons (BSE) using an Ultra 55 Zeiss SEM. Under these imaging conditions, 90% (50%) of electrons from a metal (semiconductor) that reach the detector are BSE. Thus, we would expect contrast on the Si substrate between NWs and NPs if Pt was present because of the difference in atomic number between Pt and Si. There is no discernible contrast on the bare Si substrate between NWs in Figure 5a and between NPs in Figure 5b, indicating the absence of Pt on Si(001). Yet, contrast can be observed on NW surfaces in Figure 5a. Again we would expect to see Z contrast between Pt and ErSi$_{2-x}$ and the contrast on the NW surface is indicative of Pt clusters on NW surfaces.

STM, SEM, and AFM images, as well as the areal density of Pt deposited on ErSi$_{2-x}$/Si(001) surfaces, indicate that Pt clusters preferentially aggregate on ErSi$_{2-x}$ NWs rather than the Si(001) substrate. This phenomenon of preferential aggregation is not unique to this material system. Au and Ag deposited on phase-separated diblock copolymers preferentially decorate one phase of the phase-separated polymer surface instead of randomly distributing on both phases. Preferential aggregation was attributed to differences in interfacial energy as well as differing atomic surface diffusivity of the metal atoms on the two diblock copolymer phases. These results were predicted in Monte Carlo simulations and observed experimentally in transmission electron microscopy images.[28,29]

The morphology of nanostructures after RIE is altered by Pt deposition; the size and shape of NPs in Figure 3d, that
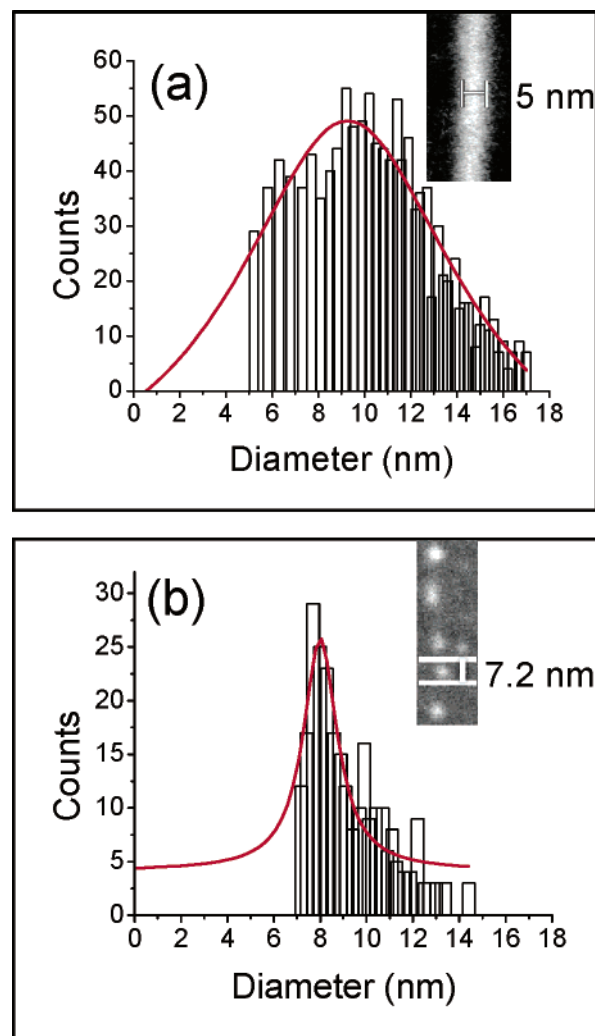

Figure 6. Histograms of calculated size distribution resulting from image analysis of the SEM images of Figure 2a and d. The mean size is 9.3 ± 5.9 nm and 8.0 ± 0.9 nm, respectively. On the basis of the resolution of SEM images under the operating conditions, the cutoff is 5 nm in Figure 6a and 7.2 nm in Figure 6b.

is, Pt/ErSi$_{2-x}$/Si(001) with 0.08 ML of Pt, appears more uniform than those in Figure 3a, that is, a ErSi$_{2-x}$/Si(001) surface without Pt. Using Fovea Pro, the surface area of each NP observed in SEM images was calculated. A spherical particle shape is assumed from which the particle diameter was then calculated. These size distributions were fitted with a Lorentzian distribution function in order to obtain a full width at half-maximum (fwhm) and thereby the variation about the mean NP size. Using this method to analyze the SEM image of Figure 3a, the mean feature size was calculated as 9.3 nm in diameter and the calculated fwhm is 11.8 nm, which corresponds to a size variation ±63.4% of mean diameter as shown in Figure 6a. The size distribution from the SEM image of Figure 3d is shown in Figure 6b. The mean feature size is calculated as 8 nm, and the calculated fwhm is 1.8 nm, which corresponds to a size variation of ±11.3% of the mean diameter over an area of 1 μm^2. Data below the resolution limit of the SEM was discarded. The insets of Figure 6 show the resolution limit of the SEM under the operating conditions. The NP size

distribution is much smaller for the Pt/ErSi$_{2-x}$/Si(001) sample versus the ErSi$_{2-x}$/Si(001) sample. The areal density of NP arrays in the SEM images of Figure 3a and d was calculated as approximately 5×10^{10}/cm^2. Other material systems can form NPs via strained epitaxy and have a similar island density, but the mean diameter of these NPs is approximately 20 nm with a size variation of $\pm 17.5\%$ of mean in the InAs/GaAs system[30] and 55 nm with a size variation of $\pm 16\%$ of mean in the Ge/Si system.[31] Pt/ErSi$_{2-x}$ core−shell NPs are comparable in diameter to Pt NPs fabricated in solution and deposited on a surface using the Langmuir−Blodgett (LB) technique. The mean size and the distribution for LB assembled Pt NPs is 9.1 nm $\pm 7\%$ over an area of 0.5 μm^2.[32] Solution-phase synthesis of NPs offers tight control of mean NP size because of the presence of capping reagents. In the case of Pt/ErSi$_{2-x}$ core−shell NPs, STM images indicate that Pt clusters form on NW surfaces with a specific planar configuration,[23] possibly to maintain the lowest strain energy between Pt clusters and the ErSi$_{2-x}$ lattice. According to density functional theory calculations, the energetics that governs the preferred intra-atomic spacing in a Pt cluster and the spatial configuration is dependent on the number of atoms in a Pt cluster, that is, the cluster size.[33] The NP size will be related to the size of Pt clusters on NW surfaces because Pt is a more resistant etch mask than ErSi$_{2-x}$. Energetically preferred planer structures are a possible explanation for the narrow size distribution, that is, Pt atoms decorate the ErSi$_{2-x}$ surface at low Pt coverage with a preferred cluster size because of a similar intra-atomic spacing in the Pt cluster and the ErSi$_{2-x}$ hexagonal lattice.

We have demonstrated the ability to select NW arrays (higher coverage) or NP arrays (lower coverage) as a function of Pt coverage. The preferential aggregation of Pt on ErSi$_{2-x}$ NWs may be attributed to differences in the surface energy and atomic mobility of Pt atoms on ErSi$_{2-x}$ NWs as compared to the Si(001) surface. At low Pt coverage, regular NP arrays having a mean size of 8 nm and a size distribution of ± 0.9 nm around the mean were obtained. The mean size is significantly smaller and the size distribution is narrower than those in other strain-driven assembly systems. Strain between Pt clusters and the ErSi$_{2-x}$ lattice is a probable mechanism for forming NP arrays with a narrow size distribution. We also have preliminary data that this process is translatable to Au on DySi$_{2-x}$/Si(001) NWs.[24] Future work will involve developing this process for other noble metals such as Au, Ag, and Pd to fabricate a variety of nanostructures with different material systems. Monodisperse and highly dense metallic NP and NW arrays that are immobile on a substrate are an important precursor to generate devices with uniform response because both optical and catalytic properties are dependent on particle size and shape. The fabrication process presented here allows for good control of feature size without lithography, and thus it is a promising route to generate NP and NW arrays using a low-cost, high-throughput technique.

References

(1) Mie, G. *Ann. Phys.* **1908**, *4*, 377−445.
(2) Gans, R. *Ann. Phys.* **1912**, *37*, 881−900.
(3) Su, K. H.; Wei, Q. H.; Zhang, X.; Mock, J. J.; Smith, D. R.; Schultz, S. *Nano Lett.* **2003**, *3*, 1087−1090.
(4) Moskovits, M. *Rev. Mod. Phys.* **1985**, *57*, 783−826.
(5) Cao, Y. W. C.; Jin, R. C.; Mirkin, C. A. *Science* **2002**, *297*, 1536−1540.
(6) Grunes, J.; Zhu, J.; Anderson, E. A.; Somorjai, G. A. *J. Phys. Chem. B* **2002**, *106*, 11463−11468.
(7) Grunes, J.; Zhu, J.; Yang, M. C.; Somorjai, G. A. *Catal. Lett.* **2003**, *86*, 157−161.
(8) Gonzalez, M. J.; Peters, C. H.; Wrighton, M. S. *J. Phys. Chem. B* **2001**, *105*, 5470−5476.
(9) Casado-Rivera, E.; Volpe, D. J.; Alden, L.; Lind, C.; Downie, C.; Vazquez-Alvarez, T.; Angelo, A. C. D.; Disalvo, F. J.; Abruna, H. D. *J. Am. Chem. Soc.* **2004**, *126*, 4043−4049.
(10) Park, K. W.; Ahn, K. S.; Nah, Y. C.; Choi, J. H.; Sung, Y. E. *J. Phys. Chem. B* **2003**, *107*, 4352−4355.
(11) Huang, J. J.; Yang, H.; Huang, Q. H.; Tang, Y. W.; Lu, T. H.; Akins, D. L. *J. Electrochem. Soc.* **2004**, *151*, A1810−A1815.
(12) Villullas, H. M.; Mattos-Costa, F. I.; Bulhoes, L. O. S. *J. Phys. Chem. B* **2004**, *108*, 12898−12903.
(13) Ranganathan, E. S.; Bej, S. K.; Thompson, L. T. *Appl. Catal., A* **2005**, *289*, 153−162.
(14) Iwasa, N.; Kudo, S.; Takahashi, H.; Masuda, S.; Takezawa, N. *Catal. Lett.* **1993**, *19*, 211−216.
(15) Preinesberger, C.; Becker, S. K.; Vandré, S.; Kalka, T.; Dähne, M. *J. Appl. Phys.* **2002**, *91*, 1695−1697.
(16) Nogami, J.; Liu, B. Z.; Katkov, M. V.; Ohbuchi, C.; Birge, N. O. *Phys. Rev. B* **2001**, *63*, 233305−233308.
(17) He, Z.; Stevens, M.; Smith, D. J.; Bennett, P. A. *Appl. Phys. Lett.* **2003**, *83*, 5292−5294.
(18) Liu, B. Z.; Nogami, J. *Nanotechnology* **2003**, *14*, 873−877.
(19) Lee, D.; Lim, D. K.; Bae, S. S.; Kim, S.; Ragan, R.; Ohlberg, D. A. A.; Chen, Y.; Williams, R. S. *Appl. Phys. A* **2005**, *80*, 1311−1313.
(20) Ragan, R.; Chen, Y.; Ohlberg, D. A. A.; Medeiros-Ribeiro, G.; Williams, R. S. *J. Cryst. Growth* **2003**, *251*, 657−661.
(21) Chen, Y.; Ohlberg, D. A. A.; Medeiros-Ribeiro, G.; Chang, Y. A.; Williams, R. S. *Appl. Phys. A* **2002**, *75*, 353−361.
(22) Chen, Y.; Ohlberg, D. A. A.; Williams, R. S. *J. Appl. Phys.* **2002**, *91*, 3213−3218.
(23) Ragan, R.; Kim, S.; Li, X.; Williams, R. S. *Appl. Phys. A* **2005**, *80*, 1339−1342.
(24) Ragan, R.; Kim, S.; Chen, Y.; Li, X.; Williams, R. S. *Proc. SPIE* **2004**, *5593*, 167−172.
(25) Lee, D.; Kim, S. *Appl. Phys. Lett.* **2003**, *82*, 2619−2621.
(26) Itoh, H.; Narui, S.; Sayama, A.; Ichinokawa, T. *Phys. Rev. B* **1992**, *45*, 11136−11142.
(27) Goldstein, J.; Newbury, D. E.; Joy, D. C.; Lyman, C. E.; Echlin, P.; Lifshin, E.; Sawyer, L. C.; Michael, J. R. *Scanning Electron Microscopy and X-ray Microanalysis*, 3rd ed.; Plenum Press: New York, 2003; p 75.
(28) Gopinathan, A. *Phys. Rev. E* **2005**, *71*, 041601−041609.
(29) Lopes, W. A. *Phys. Rev. E* **2002**, *65*, 031606−031614.
(30) Leonard, D.; Pond, K.; Petroff, P. M. *Phys. Rev. B* **1994**, *50*, 11687−11692.
(31) Kamins, T. I.; Carr, E. C.; Williams, R. S.; Rosner, S. J. *J. Appl. Phys.* **1997**, *81*, 211−219.
(32) Song, H.; Kim, F.; Connor, S.; Somorjai, G. A.; Yang, P. D. *J. Phys. Chem. B* **2005**, *109*, 188−193.
(33) Yang, S. H.; Drabold, D. A.; Adams, J. B.; Ordejon, P.; Glassford, K. *J. Phys. Condens. Matter* **1997**, *9*, L39-L45.

NL060640L